JOURNAL OF SOLID STATE CHEMISTRY 100, 313–324 (1992)

Characterization of $TaFe_{1.25}Te_3$, a New Layered Telluride with an Unusual Metal Network Structure

M. E. BADDING, J. LI, AND F. J. DISALVO*

Department of Chemistry, Cornell University, Ithaca, New York 14853

AND W. ZHOU AND P. P. EDWARDS†

University Chemical Laboratory, Lensfield Road, Cambridge CB2 1EW, England

Received September 26, 1991; in revised form March 30, 1992; accepted March 31, 1992

The new layered material, $TaFe_{1+x}Te_3$ ($0.25 < x < 0.29$), has been synthesized by reaction of the constituent elements. Single-crystal X-ray diffraction studies show that at $x = 0.25$ the compound crystallizes in the space group $P2_1/m$ (no. 11) ($a = 7.436(1)$, $b = 3.638(1)$, $c = 10.008(1)$ Å, $\beta = 109.17(1)°$). The structure features an unusual Ta–Fe bonded network that contains an equal number of Ta and Fe atoms. The metal network lies between tellurium layers, forming a $FeTaTe_3$ "sandwich." Additionally, x Fe atoms per formula unit partially occupy a square pyramidal site that provides interlayer bonding through the apical tellurium, which is in an adjacent "sandwich." Selected area electron diffraction studies did not reveal any order in the partially occupied Fe positions. Electrical and magnetic measurements reveal that, at $x = 0.25$, the compound is an antiferromagnetic metal ($T_N = 200$ K) and undergoes a structural phase transition at 1010 K.

Introduction

Ternary niobium and tantalum tellurides show great promise for the synthesis of interesting new materials. The binary and ternary sulfides and selenides of this group show many examples of novel electronic behavior, including charge-density waves (*1–3*), superconductivity (*4–7*), and anisotropic electrical and optical properties (*8*), as well as important intercalation chemistry (*9, 10*), and interesting structural chemistry including mixed-metal-network layered compounds (*11–16*), misfit layer compounds (*17*), and other novel low-dimensional structures (*18, 19*).

The short list of well-characterized ternary tellurides (*20–29*) shows examples of novel low-dimensional structural types. Compounds recently synthesized in our laboratory, $M_4M'Te_4$ (M = Nb,Ta; M' = Cr,Fe,Co,Ni,Al,Si) (*27*) and $NbMTe_2$ (M = Co,Fe) (*29*) display unusual metal networks which, owing to the greater covalency of the metal–tellurium bond and resulting propensity to form metal–metal bonds, indicate that the chemistry of the telluride phases will be quite different from that of the sulfides and selenides.

* To whom correspondence should be addressed.

† Present address: School of Chemistry, University of Birmingham, Edgebaston, Birmingham, England BIS 2TT.

0022-4596/92 $5.00

In this paper we report the structure and electronic properties of $TaFe_{1.25}Te_3$, an unusual layered material which contains a tantalum–iron mixed-metal network and a partially occupied iron site. Resistivity and susceptibility measurements show the compound to be an antiferromagnetic metal with $T_N = 200$ K, which undergoes a phase transition (probably structural) at 1010 K.

Sample Preparation

Powder samples were synthesized by direct combination of the elements. An appropriate mixture of tantalum powder (Strem, 99.8%), iron powder (Matthey, 99.999%), and tellurium powder (Alfa, 99.999%) was sealed under vacuum in a quartz tube and heated from room temperature to 775°C over a period of 24 hr, left at 775°C for 3 days, and then cooled in the furnace with the power off. To ensure complete reaction, the samples were ground under Ar, pressed into a pellet, sealed in an evacuated quartz tube, and heated at 775°C for 5 more days.

Single crystals used in the structure determination below were grown by chemical vapor transport. A 1-g stoichiometric mixture of the elements and 10 mg $TeCl_4$ (transporting agent) were sealed in an evacuated 6-inch-long 10-mm ID quartz tube. The tube was placed in a furnace and slowly heated to temperature with the hot end at 690°C and the cool end at 660°C. The needle-shaped crystals, which grow up to 1 cm in length, form in the cool zone. After 1 week, the furnace was shut off and the tube removed after allowing the furnace to cool to room temperature.

Structure Determination and Stoichiometry Analysis

Qualitative microprobe analysis of the single crystals (Energy Dispersive) showed only the presence of tantalum, iron, and tellurium.

The iron content of single crystals was analyzed by the Inductively Coupled Plasma atomic emission method. Two crystals weighing in total 15.32(3) mg were digested in 5 ml of 5 : 1 (conc. HCl):(30% H_2O_2) and diluted to 100.0(1)[1] ml. The iron concentration was determined from the emission line at 259.9 nm to be 17.0(1) μg/ml, which gives 11.1(1)% by weight iron in the crystals.

Weissenberg photos revealed approximate cell constants and a monoclinic cell symmetry. Single crystal intensity data were collected on a well-formed crystal using a Syntex $P2_1$ diffractometer. An automatic indexing algorithm indicated a primitive monoclinic cell. Cell constants were refined by centering on 25 reflections above 15° 2Θ. Cell and data collection parameters are listed in Table I. An analytical absorption correction was applied to the data after identifying and carefully measuring the crystal faces. All of the measured $0k0$ reflections $\{k:0\text{–}5\}$ showed intensity greater than three times their esd (estimated standard deviation) only for odd k, consistent with a 2_1 screw axis along b. The structure was solved by direct methods and refined, using SHELXTL PLUS Rel. 4.11 software (Siemens), in the centrosymmetric space group $P2_1/m$ (no. 11). Once the bulk of the electron density (one tantalum, one iron, and three tellurium atoms all lying in $2e$ sites) was accounted for, the R factors for an isotropic refinement of the data were quite good, considering the elements present, with $R = 3.8\%$, $R_w = 4.0\%$, and GOF = 2.96.[2] There remained one significant peak in the difference Fourier map. This electron density was well modeled by partial occu-

[1] Estimated deviations and uncertainties in the last significant figure of a reported number are indicated in parenthesis throughout the article.

[2] $R = \Sigma||F_o| - |F_c||/\Sigma|F_o|$; $R_w = [\Sigma w(|F_o| - |F_c|)^2)/\Sigma wF_o^2]^{1/2}$; GOF $= [w(|F_o| - |F_c|)^2/(n_o - n_v)]^{1/2}$, where n_o = no. of obs. reflections, and n_v = no. of variables.

TABLE I

CRYSTAL DATA, DATA COLLECTION, AND REFINEMENT PARAMETERS OF $TaFe_{1.25}Te_3$

Crystal data	
Empirical formula	Fe1.25TaTe3
Color, Habit	Metallic, plate
Crystal size (mm3)	0.18 × 0.07 × 0.01
Crystal system, space group	Monoclinic, $P2_1/m$
Unit cell dimensions (Å)	a = 7.436(1)Å
	b = 3.638(1)Å
	c = 10.008(1)Å
	β = 109.17(1)°
Volume (Å^3)	255.73(8)
Z	2
Density (calculated, g/cc)	8.228
Absorption coeff, μ (mm^{-1})	41.32
Data collection	
Diffractometer used	Syntex $P2_1$
Radiation	Mo-$K\alpha$ (λ = 0.71073 Å)
Monochromator	Highly oriented graphite crystal
2θ Range	3.0–65.0°
Scan type	$\theta - 2\theta$
Octants measured	$\pm h \pm k \pm l$
Reflections collected	4281
Independent reflections	1062 (R_{int} = 3.2%)
Observed reflections	1032 [$F > 3.0\ \sigma(F)$]
Min/Max transmission	0.086/0.745
Refinement	
Refinement method	Full-matrix least-squares
Quantity minimized	$\Sigma_w(F_0 - F_c)^2$
Extinction correction[c]	χ = 0.00055(8)
Number of parameters refined	38
Final R indices (observed data)	R^a = 2.15%, $R_w{}^b$ = 2.79%
Goodness-of-fit	1.64
Largest and mean Δ/σ	0.002, 0.001
Data-to-parameter ratio	27.2 : 1
Largest difference peak	1.68, −2.15 eÅ^{-3}

[a] $R = \Sigma(|F_0| - |F_c|)/\Sigma(|F_0|)$.
[b] $R_w = [\Sigma w(|F_0| - |F_c|)^2)/\Sigma(w|F_0|^2)]^{1/2}$; $w = 1/(\sigma^2(F) + 0.0001 * F^2)$.
[c] Where $F_c^* = F_c(1 + 0.002\chi F_c^2/\sin(2\theta))^{-1/4}$.

pancy of a 2*e* site by an iron atom (Fe2), and brought the residual factors down to R = 3.0%, R_w = 3.4%, and GOF = 2.4, with the occupancy factor refined to 0.13(1) iron atom. This occupancy would imply a stoichiometry of $TaFe_{1.13}Te_3$ which corresponds to 10.1% by weight iron, significantly less than that indicated by ICP analysis (11.1(1)%). Additionally, a careful powder diffraction analysis, discussed below, indicates the stoichiometry of the compound is $TaFe_{1.25}Te_3$. This formula is also consistent with the ICP data—the calculated weight percent iron is 11.1%. Apparently, since the iron atom in the partially occupied site contributes only a relatively small amount to the total X-ray scattering of the compound, an accurate refinement of the occupancy factor is not possible. Even with zero occupancy of the partially occupied site the re-

TABLE II

ATOMIC (FRACTIONAL) COORDINATES AND EQUIVALENT ISOTROPIC DISPLACEMENT COEFFICIENTS ($Å^2 \times 10^3$) FOR $TaFe_{1.25}Te_3$

Atom	Site	x	y	z	U(eq)[a]
Ta1	2e	0.8340(1)	0.25	0.3007(1)	10.6(1)
Fe1	2e	0.6147(2)	−0.25	0.0890(1)	12.0(3)
Fe2[b]	2e	0.7686(11)	0.25	−0.0047(7)	47.7(27)
Te1	2e	0.4392(1)	0.25	0.1860(1)	12.6(1)
Te2	2e	0.9835(1)	−0.25	0.1589(1)	11.6(1)
Te3	2e	0.2179(1)	0.25	0.4970(1)	10.7(1)

[a] Equivalent isotropic U defined as one-third of the trace of the orthogonalized U_{ij} tensor.
[b] Occupancy fraction fixed at 0.25.

sidual factors given above are quite low. Since, in this case, the chemical analysis is more likely an accurate indication of the true stoichiometry the occupancy fraction of the Fe2 site was fixed at 0.25.

Fixing the occupancy factor of the Fe2 site at the higher value of 0.25 resulted in slightly higher residuals (R = 3.09%, R_w = 3.41%, and GOF = 2.51) and an increase in the Fe2 thermal parameter (from 0.009(3) to 0.044(2) $Å^2$). Since the occupancy factor and thermal parameters are highly correlated, it is not clear whether this significantly higher thermal parameter for Fe2 is real. Additionally fixing the Fe2 thermal parameter at 0.013 $Å^2$ (similar to the other iron atoms) significantly increased the residuals to R = 3.58%, R_w = 3.97%, and GOF = 3.09. In the later stages of refinement, the Fe2 thermal parameter was allowed to refine. Employing an empirical extinction correction and anisotropic thermal parameters gave final residuals of R = 2.15%, R_w = 2.79%, and GOF = 1.64. The analytical forms of the scattering factor tables for the neutral atoms were used (*30*) and all scattering factors were corrected for both real and imaginary components of anomalous dispersion (*31*). Relevant cell, data collection, and refinement parameters are listed in Table I. Atomic coordinates are listed in Table II. Bond Lengths and Angles are listed in Table III.

A powder diffraction study was undertaken in order to investigate whether the partial occupancy leads to a range of stable iron stoichiometries, as might be expected. A series of reactions with the formula $TaFe_{1+x}Te_3$ were carefully prepared as described above, and examined by X-ray powder diffraction using a Scintag XDS-2000 diffractometer with an Li–Ge detector. Several resulting powder patterns are displayed in Fig. 1. Peaks due to the presence of second phases are observed for stoichiometries below x = 0.25 and above x = 0.29; on the iron-poor side $TaTe_2$ is present as indicated by the peak at 31.31° 2θ (*32*), and on the iron-rich side another, as yet unidentified, phase is indicated by the peak at 11.20° 2θ. In order to better quantify the iron stoichiometry, as determined by powder diffraction, the intensity of the primary $TaTe_2$ diffraction peak (31.31° 2θ) relative to the intensity of the primary $TaFe_{1.25}Te_3$ peak

TABLE III

SELECTED INTERATOMIC DISTANCES AND ANGLES FOR $TaFe_{1.25}Te_3$

Fe1–2Fe1	2.720(1)	Te2–Fe1–2Te1	120.9(1)
Fe1–2Fe2	2.490(6)	Te1b–Fe1–2Te1	117.6(1)
Fe1–Fe2c	2.694(8)	Te2–Fe1–Te1b	93.8(1)
Fe1–2Ta	2.861(1)	Te1–Fe1–Te1a	88.6(1)
Fe1–2Te1	2.605(1)		
Fe1–Te1b	2.647(1)		
Fe1–Te2	2.598(1)		
Fe2–Ta	2.933(7)	Te2′–Fe2–2Te4	87.8(2)
Fe2–2Te1	2.673(5)	Te1′–Fe3–2Te6	88.1(2)
Fe2–2Te2	2.612(5)	Te4–Fe3–Te4a	85.9(2)
Fe2–Te2′	2.766(9)	Te4–Fe3–Te6	92.8(1)
		Te6–Fe3–Te6a	88.1(2)
Ta1–Te2	2.775(2)	Te2–Ta1–2Te3	85.7(1)
Ta1–2Te3	2.840(2)	Te2–Ta1–2Te6	109.6(1)
Ta1–Te5	2.888(2)	Te2–Ta1–Te5	163.1(1)
Ta1–2Te6	2.753(2)	Te3–Ta1–Te6	96.6(1)
		Te3–Ta1–Te3a	79.7(1)
		Te6–Ta1–Te6a	82.7(1)
Shortest Te–Te contacts:			
Intralayer: Te#–Te# along b-axis			3.638(1)
Interlayer: Te2–Te2′			3.741(1)

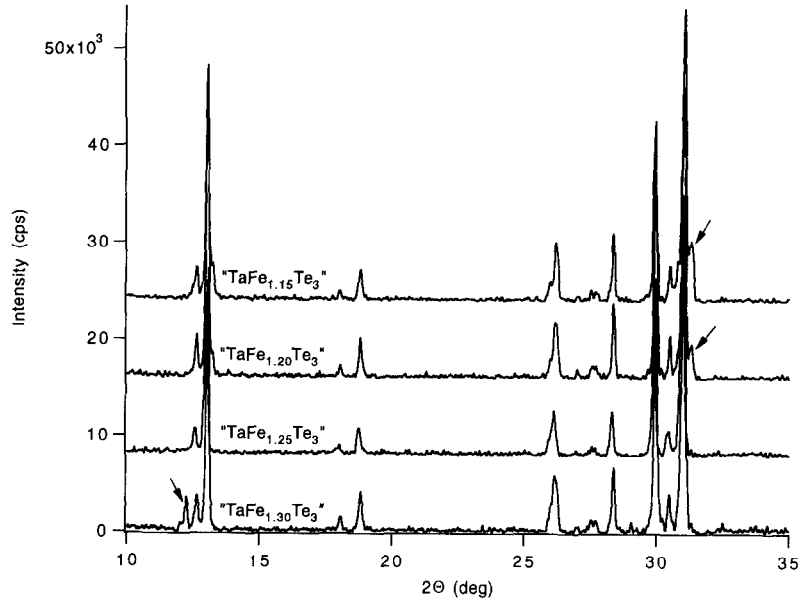

FIG. 1. Powder diffraction spectra of the stoichiometry series $TaFe_{1+x}Te_3$ for $0.15 < x < 0.30$. Spectra for $x < 0.25$ and $x \geq 0.29$ show second-phase peaks.

(31.02° 2θ) was determined as a function of iron stoichiometry for $x < 0.25$. Peaks were deconvoluted using Scintag Graphics Package v. 2.50. As seen in Fig. 2, a linear extrapolation of the intensity ratio reaches zero, or no second phase present, at a stoichiometry very close to 1.25. On the iron-rich side, reaction mixtures with iron stoichiometry up to 1.29 showed no second phase present, indicating a small range (1.25 to 1.29) of stability in the iron stoichiometry. The powder study clearly indicates a minimum iron stoichiometry of 1.25—in good agreement with ICP data as mentioned above.

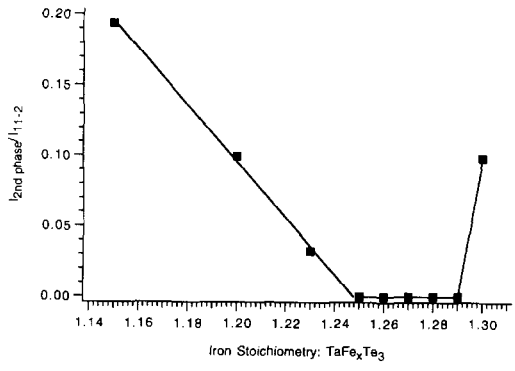

FIG. 2. Plot of relative intensity of second phase peak vs iron stoichiometry.

In order to study the magnetic structure and the high temperature phase transition (*vide infra*), we have undertaken a powder neutron diffraction study. Although the details will be published separately, we note that the large neutron scattering length of Fe relative to Ta and Te allows a more precise determination of the occupancy of the 2e Fe atom. A refinement of neutron powder data taken at room temperature gives an iron stoichiometry of 1.24(1), as expected from the chemical analysis and X-ray powder diffraction. This indicates the difficulty of determining stoichiometry from single crystal X-ray diffraction alone—especially for elements with scattering factor small relative to other elements present.

The possible existence of a superstructure, which might be expected considering the narrow range of stability of the phase, was investigated by careful examination of the X-ray powder pattern of $TaFe_{1.25}Te_3$, as well as strongly overexposed X-ray single crystal oscillation and Weissenberg photos, all of which showed no evidence of superlattice lines. A careful search for weak superlattice reflections using the Syntex $P2_1$ (graphite monochromator and scintillation detector with pulse height analyzer) also failed to give any indication of a superlattice. Mindful that the comparatively weak X-ray scattering power of iron relative to tantalum or tellurium might make elucidation of a superstructure by X-ray diffraction difficult in this particular case, we decided to employ Transmission Electron Microscopy to investigate the structure more sensitively and at a more local level.

TEM Analysis

A polycrystalline sample of $TaFe_{1.25}Te_3$ was analyzed using a JEOL-200x transmission electron microscope (TEM) in which a ±45° double-tilt specimen stage was used. Selected Area Electron Diffraction (SAED) patterns obtained from the sample are displayed in Fig. 3 which shows diffraction from the $a^* - b^*$ and $b^* - c^*$ reciprocal lattice planes. All SAED patterns collected on the sample were consistent with the primitive monoclinic cell used in the X-ray diffraction work; no indication of a superlattice was found.

The SAED patterns do show an unexpectedly large intensity for the (010) reflection, which may indicate the 2_1 symmetry is broken on a microscale—no (0k0) reflections for k odd were observed in the single-crystal X-ray diffraction experiment. Dynamical scattering effects can, however, lead to observation of reflections not allowed by kinematical theory.

Description of the Structure

A view down the monoclinic axis (Fig. 4) clearly shows the ribbon-like nature of the main metal network (Ta–Fe1–Fe1–Ta), which is bound on both sides by tellurium atoms (Te1, Te2, Te3) and by the partially occupied iron site (Fe2). Fe2 also forms an interlayer (Fe2–Te2′) bond of 2.76 Å. Adjacent "ribbons" are linked together by bridging tellurium atoms (Te3) to form $TaFeTe_3$ sandwiches which are stacked perpendicular to the [1 0 −1] direction.

A view nearly perpendicular to the (1 0 −1) plane (Fig. 5) shows the nature of the bonding in the layer. Ta is coordinated by a distorted octahedron of tellurium atoms, by two iron atoms in the ribbon-like metal network, and by the partially occupied (Fe2) site. Fe1 is coordinated by a distorted tetrahedron of tellurium atoms, by a distorted rectangle of two tantalum and two iron atoms in the ribbon, and by three Fe2 sites. As seen in Fig. 6, Fe2 is coordinated in a square-pyramidal fashion by tellurium, and additionally is bonded to the rectangular metal moiety (Fe1 × 3, and Ta).

The Fe–Fe distance within the metal ribbon (2.722 Å) is somewhat longer than the Fe–Fe distance in iron metal (2.54 Å), but still indicates an important interaction. The Fe–Ta distance of 2.860 Å is comparable to the sum of the covalent radii (2.70 Å), and indicates metal–metal bonding. The Fe–Te bond lengths range from 2.575–2.674 Å, which is similar to values found in other ternary tellurides; iron–tellurium distances in the recently discovered compound $NbFeTe_2$, for example, range from 2.542–2.610 Å (*29*). The Ta–Te distances range from 2.753–2.888 Å, similar to distances in $TaTe_2$, which range from 2.663–2.923 Å (*33*). The closest Te–Te contact is 3.638 Å (b-axis length) between Te atoms of the same type. The closest interlayer contact is 3.742 Å between Te2 and Te2′, which is typical of layered tellurides;

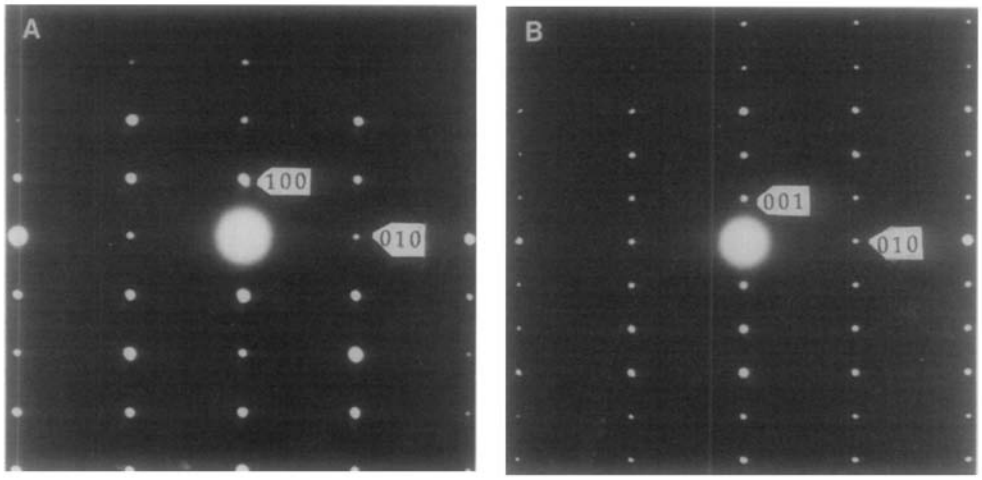

FIG. 3. Select area electron diffraction photos of $TaFe_{1.25}Te_3$. Photo (A) shows the $a^* - b^*$ plane; photo (B) shows $b^* - c^*$. Both photos are consistent with the reported monoclinic cell.

interlayer Te–Te distances in $TaTe_2$ range from 3.527 to 3.999 Å (*33*).

Magnetic Susceptibility

The magnetic susceptibility of a polycrystalline sample was measured by the Faraday method from 4.2 to 1130 K (*34*) and is plotted in Fig. 7. The susceptibility was found to be field-independent, indicating no appreciable ferromagnetic impurity. $TaFe_{1.25}Te_3$ shows a sharp antiferromagnetic transition with $T_N = 200$ K. Above 450 K, the susceptibility fits the Curie–Weiss expression $\chi_g = C_g/(T + \Theta) + \chi_0$, where C_g is the Curie constant, Θ the Weiss temperature, and χ_0 a temperature-independent term. A normalized least-squares fit (*35*) of the data from 450 to 1000 K gives values for the Curie–Weiss parameters as listed in Table IV. The goodness of fit, ε, is estimated by the root mean square fractional deviation of the data from the above form. Below 450 K, the susceptibility data fall below the extrapolated Curie–Weiss fit.

An effective moment of 3.7 Bohr magnetons per iron atom is obtained from the Curie constant, which is a lower than expected for iron localized high-spin Fe^{2+} (4.9 μ_B) or Fe^{3+} (5.9 μ_B). The low moment per iron in this compound might suggest that not all the irons are magnetic, and/or the expected high degree of covalency of the bonding reduces the iron moment. If the Fe2 atoms are not magnetic, an effective moment of 4.2 μ_B per iron, still considerably below the spin-only value, is obtained. If the Fe2 atoms are magnetic, then the sharpness of the antiferromagnetic transition suggests that the Fe2 atoms may be at least locally ordered.

Interestingly, the Weiss temperature of −218K indicates that the dominant exchange interaction is *ferro*magnetic. One possible model which would account for this behavior is ferromagnetic exchange between intraribbon iron atoms, which are the closest and therefore expected to have stronger exchange, and an antiferromagnetic exchange between ribbons or sandwiches.

At just over 1000 K, the susceptibility drops sharply indicating a phase transition which is first-order as cycling reveals a small

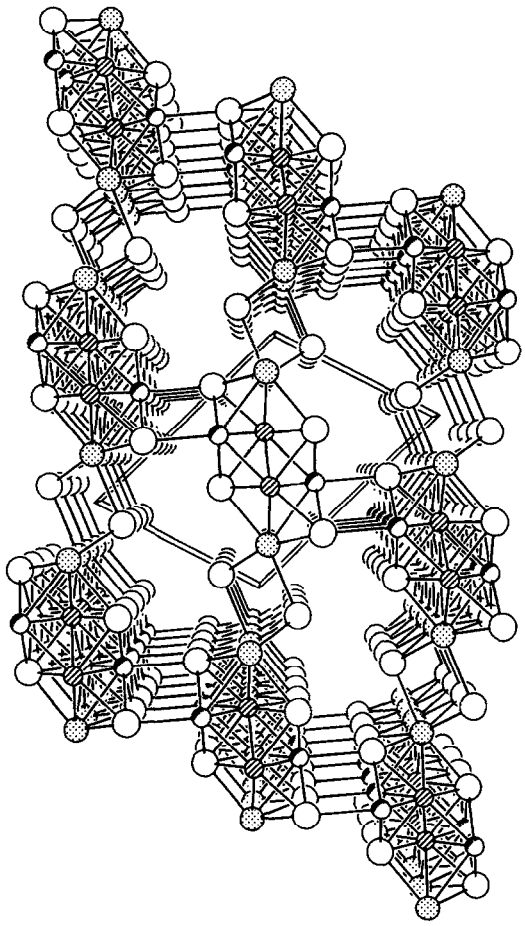

FIG. 4. View of the structure looking down the *b* axis. Dotted circles, tantalum; fully hatched circles, iron (Fe1); partially hatched circles, partially occupied iron (Fe2); open circles; tellurium.

hysteresis (see inset on Fig. 7). The magnitude of the change in susceptibility at the transition (1×10^{-6} emu/g) is significant when compared to χ_0 (-0.4×10^{-6} emu/g) and indicates that the transition involves either a change in the iron moment or a change in the exchange interactions.

Electrical Resistivity

The temperature dependence (4.2–300 K) of the electrical resistivity of a large needle-like single crystal ($0.3 \times 0.9 \times 10.0$ mm^3) was measured along a direction parallel to the *b*-axis using the standard four-probe technique. Indium contacts were made using an ultrasonic soldering iron, and were found to display ohmic behavior. The results are displayed in Fig. 8. The room-temperature resistivity is about 4×10^{-4} ohm-cm and only 1.5 times greater than the resistivity at 4.2 K, which indicates $TaFe_{1.25}Te_3$ is a poor metal with strong scattering. The accelerated drop in resistivity near 200 K may be associated with the ordering of the magnetic moments.

Discussion

$TaFe_{1.25}Te_3$ is quite different from typical layered chalcogenides, which usually consist of metal atoms occupying holes between close-packed anion layers. The position of the tellurium atoms in this phase cannot be derived by a small distortion of close-packed layers. Looking at Fig. 5, one can see that the rows of Te atoms running parallel to the *b*-axis which bind between ribbons (Te3) have, on both sides, neighboring Te atom rows which are shifted with respect to the initial row; this gives Te3 six nearly equidistant neighbors as is characteristic of a close-packed layer. The Te atoms which bind between ribbons (Te1, Te2), however, have one neighboring row shifted and one not shifted, which leads to an unusual, asymmetric packing. Formation of the metal ribbon forces the formation of an irregular anion layer.

The structure can be more fruitfully described in terms of linking metal-centered tellurium polyhedra. $TaFe_{1.25}Te_3$ is structurally related to other mixed-metal-network layered ternary tantalum chalcogenides, including Ta_2NiX_5 (X = S, Se) (*16*). The structure of Ta_2NiX_5 can be described as layers of edge-sharing Ta-centered chalcogenide octahedra which distort to include a chain of edge-sharing Ni-centered tetrahedra re-

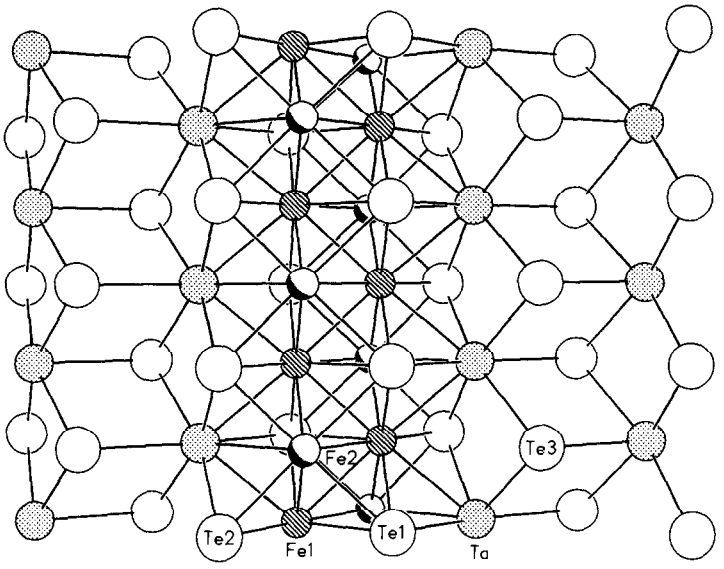

FIG. 5. View nearly perpendicular to the (1 0 −1) plane shows coordination environments in the layer.

sulting in Ta–Ni–Ta ribbons which are bridged in the same manner as the Ta–Fe–Fe–Ta ribbons described here. The relationship between the structures is simply the addition of another chain of edge-sharing tetrahedra, which in this case are Fe-centered.

The proclivity to form a metal–metal bonded network seems to be one of the unfolding features of telluride chemistry. Other examples include Ta_4MTe_4 (M = Si, Al, Cr, Fe, Co, Ni), which contains a one-dimensional Ta–M metal network (*27*), and $NbMTe_2$ (M = Fe,Co) (*22, 29*), which is a layered compound featuring a honeycomb Nb network which includes an M atom pair. Clearly more compounds with other unusual metal–metal networks will be found in the ternary niobium and tantalum telluride systems.

The nature of the disorder associated with the partial occupancy of the Fe2 site in this compound is puzzling. The powder diffraction study indicates $TaFe_{1.25}Te_3$ exists only for a narrow range of iron stoichiometry from 1.25 to 1.29. Since fixed compositions are usually indicative of order in transition metal compounds, random occupancy of the Fe2 site seems suspect. The sharpness

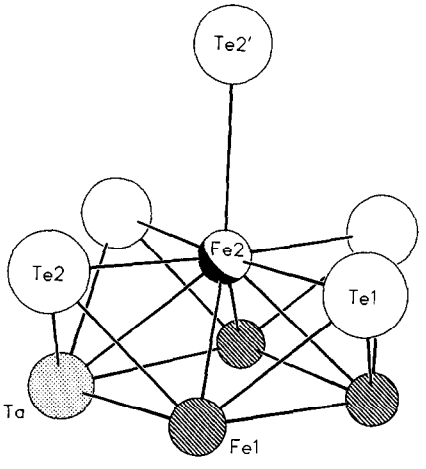

FIG. 6. Environment of the partially occupied site (Fe2).

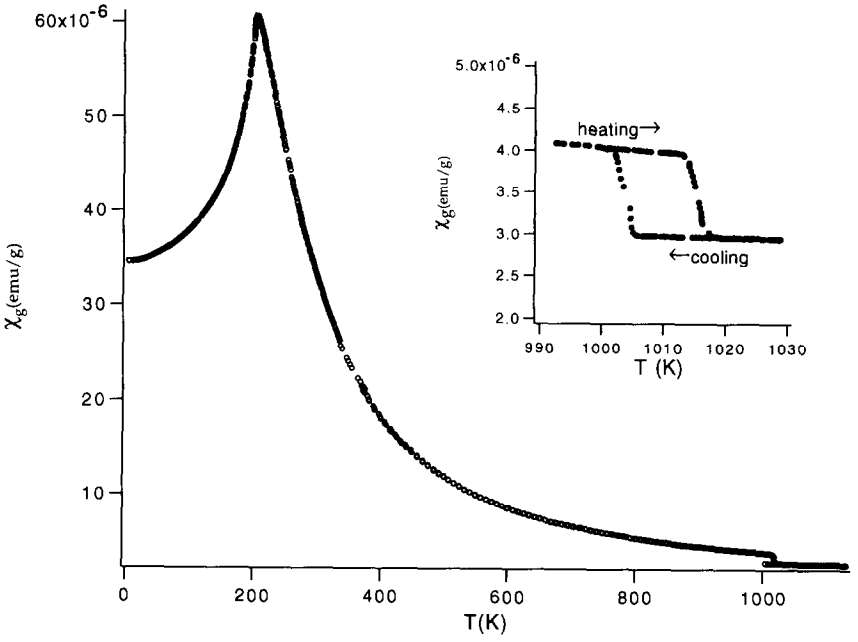

FIG. 7. Temperature dependence of the magnetic susceptibility of $TaFe_{1.25}Te_3$ (4.2–1130 K). Inset: expansion of the curve showing the phase transition near 1010 K.

of the antiferromagnetic transition in the susceptibility (Fig. 7) is another indication that the Fe2 atoms might be ordered, assuming they are magnetic. The TEM study, however, shows no evidence of any superstructure of measurable intensity.

One possibility that could account for the observed results is that the vacancies are in fact ordered on each ribbon, but that registry between ribbons is lost on a short scale. Intuitively, the energy differences associated with interribbon disorder would be small since the distances involved (>7 Å) are relatively large. Any short-range order would have to occur on a scale of a hundred angstroms or less to be consistent with the Selected Area Electron Diffraction results which, in our work, averages the structure over a scale of approximately 1000 Å.

TABLE IV

CURIE–WEISS CONTRIBUTION TO THE MAGNETIC SUSCEPTIBILITY OF $TaFe_{1.25}Te_3$; $\chi_g = C_g/(T + \Theta) + \chi_0$ FIT FROM 450 TO 1000 K

χ_0 (10^{-6} emu/g)	C_g (10^{-6} emu K/g)	Θ (K)	μ_{eff}/Fe (μB)	ε (%)
−0.4	3,400	−218	3.7	0.28

Conclusion

The new layered phase, $TaFe_{1.25}Te_3$, contains an unusual {Ta–Fe–Fe–Ta} metal–metal bonded ribbon network and a partially occupied iron site. Electrical resistivity and magnetic susceptibility measurements show the material is an antiferromagnetic metal (T_N = 200 K). The susceptibility also shows a first-order phase transition at 1010 K, which is probably structural in nature and involves a change in

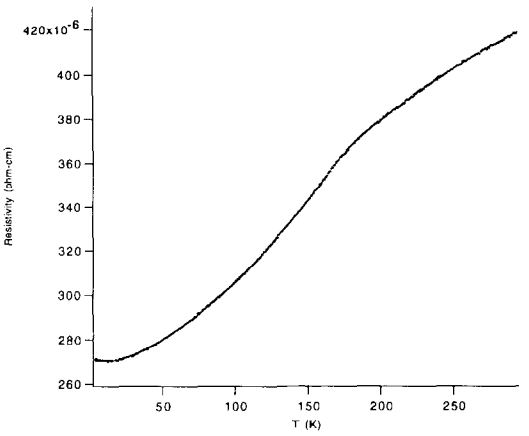

FIG. 8. Temperature dependence of the electrical resistivity of $TaFe_{1.25}Te_3$ (4.2–300 K).

either the magnetic moment or the exchange interactions.

The exact nature of the partially occupied site remains puzzling. X-ray powder diffraction experiments indicate the material has a narrow range of stability for the iron stoichiometry from $TaFe_{1.25}Te_3$ to $TaFe_{1.29}Te_3$, which corresponds to 25–29% filling of the Fe2 site. Selected Area Electron Diffraction patterns, surprisingly, show no superlattice of measurable intensity.

Other measurements, which might help elucidate the nature of the Fe2 site, would be interesting. Mössbauer spectroscopy on the ^{57}Fe nucleus would, in particular, be useful in identifying the magnetic nature of each of the iron atoms. Neutron diffraction in both the magnetic and nonmagnetic states could also be quite revealing. We are presently pursuing such experiments.

Acknowledgments

This research was supported by the Department of Energy, Division of Basic Energy Sciences, Grant DE-FG02-87ER45298 (Cornell), British Petroleum and SERC (Cambridge), and a NATO grant for travel to Cambridge.

References

1. J. A. WILSON, F. J. DISALVO, AND S. MAHAJAN, *Adv. Phys.* **24,** 117 (1975).
2. F. J. DISALVO AND T. M. RICE, *Phys. Today.* **32**(4), 32 (1979).
3. R. J. CAVA, F. J. DISALVO, M. EIBSCHUTZ, AND J. V. WASZCZAK, *Phys. Rev. B: Condens. Matter.* **27,** 7412 (1983).
4. G. K. SHENOY, B. D. DUNLAP, AND F. Y. FRADIN (Eds.) "Ternary Superconductors," Elsevier North-Holland, New York (1981).
5. E. AMBERGER, K. POLBORN, P. GRIMM, M. DIETRICH, AND B. OBST, *Solid State Commun.* **26,** 943 (1978).
6. R. F. FRINDT AND D. J. HUNTLEY, *in* "Optical and Electrical Properties" (P. A. Lee, Ed.), p. 403, Reidel, Dordrecht (1976).
7. R. SCHOLHORN AND W. SCHRAMM, Z. *Naturforsch.* **346,** 697 (1979).
8. J. A. WILSON AND A. D. YOFFE, *Adv. Phys.* **18,** 193 (1969).
9. J. ROUXEL AND R. BREC, *Annu. Rev. Mater. Sci.* **16,** 137 (1986).
10. G. HUAN AND M. GREENBLATT, *Mater. Res. Bull.* **22,** 505 (1987).
11. S. A. SUNSHINE, D. A. KESZLER, AND J. A. IBERS, *Acc. Chem. Res.* **20,** 395 (1987).
12. S. A. SUNSHINE AND J. A. IBERS, *J. Solid State Chem.* **69,** (1987).
13. P. J. SQUATTRITO, S. A. SUNSHINE, AND J. A. IBERS, *J. Solid State Chem.* **64,** 261 (1986).
14. F. J. DISALVO, C. H. CHEN, R. M. FLEMING, J. V. WASZCZAK, R. G. DUNN, S. A. SUNSHINE, AND J. A. IBERS, *J. Less-Common Met.* **116,** 51 (1986).
15. D. A. KESZLER AND J. A. IBERS, *J. Solid State Chem.* **57,** 68 (1985).
16. S. A. SUNSHINE AND J. A. IBERS, *Inorg. Chem.* **24,** 3611 (1985).
17. G. A. WIEGERS, A. MEETSMA, S. VAN SMAALEN, R. J. HAANGE, J. WULLF, T. ZEINSTRA, J. L. DE BOER, S. KUYPERS, G. VAN TENDELOO, J. VAN LANDUYT, S. AMELINCKX, A. MEERSCHAUT, P. RABU, AND J. ROUXEL, *Solid State Commun.* **70,** 409 (1989).
18. J. ROUXEL, *J. Solid State Chem.* **64,** 305 (1986).
19. M. EVAIN, M. QUEIGNEC, R. BREC, AND C. SOURISSEAU, *J. Solid State Chem.* **75,** 413 (1988).
20. G. HUAN AND M. GREENBLATT, *Mater. Res. Bull.* **22,** 943 (1987).
21. E. W. LIIMATTA AND J. A. IBERS, *J. Solid State Chem.* **71,** 384 (1987).

22. B. HUANG, B. SHANG, AND J. HUANG, *J. Jiegou Huaxue*. **7,** 133 (1988).
23. B. HUANG, B. SHANG, AND J. HUANG, *J. Jiegou Huaxue*. **7,** 214 (1988).
24. E. W. LIIMATTA AND J. A. IBERS, *J. Solid State Chem.* **77,** 141 (1988).
25. B. HUANG, B. SHANG, AND J. HUANG, *J. Jiegou Huaxue*. **8,** 145 (1989).
26. E. W. LIIMATTA AND J. A. IBERS, *J. Solid State Chem.* **78,** 7 (1989).
27. M. E. BADDING AND F. J. DISALVO, *Inorg. Chem.* **29,** 3952 (1990).
28. A. MAR AND J. A. IBERS, *J. Solid State Chem.* **92,** 352 (1991).
29. J. LI, M. E. BADDING, AND F. J. DISALVO, *Inorg. Chem.* **31,** 1050 (1992).
30. D. T. CROMER AND J. T. WABER, "International Tables for X-Ray Crystallography" Vol. IV, Table 2.2B, Kynoch Press, Birmingham, England (1974).
31. D. T. CROMER AND J. T. WABER, "International Tables for X-Ray Crystallography" Vol. IV, Table 2.3.1, Kynoch Press, Birmingham, England (1974).
32. K. SELTE, E. BJERKELUND, AND A. KJEKSHUS, *J. Less-Common Met.* **11,** 14 (1966).
33. B. E. BROWN, *Acta Crystallogr.* **20,** 264 (1966).
34. J. K. VASSILIOU, M. HORNBOSTEL, R. ZIEBARTH, AND F. J. DISALVO, *J. Solid State Chem.* **81,** 208 (1989).
35. F. J. DISALVO, J. V. WASZCZAK, AND M. EIBSCHUTZ, *Phys. Rev. B: Condens. Matter.* **24,** 5143 (1981).